Design of Variable Geometry Medium Power Hall Thruster

IEPC-2015-183/ISTS-2015-b-183

Presented at Joint Conference of 30th International Symposium on Space Technology and Science
34th International Electric Propulsion Conference and 6th Nano-satellite Symposium, Hyogo-Kobe, Japan
July 4 – 10, 2015

B.M. Plecque[1] M.W. Crofton[2] K.D. Diamant[3] R. Spektor[4] J.A. Young[5] W.A. Cox[6] A.A. Hubble[7]
The Aerospace Corporation, El Segundo, CA, 90245, United States

Abstract: A variable geometry 6kW Hall thruster was designed. The thruster has a discharge chamber outer diameter of 194mm and inner diameter of 110mm. The discharge chamber can be translated axially by 30mm. The anode translates free of the discharge chamber and can produce a chamber depth of 18mm to 58mm. The cathode can be located external to the thruster (on either side of the separatrix) or at an axially variable location in the center of the thruster. The magnetic circuit consists of ten copper wire solenoids, and allows for single, four, and eight outer coil configurations to be created. Using ANSYS Maxwell3D simulations, the maximum radial magnetic field component was found to be about 300G for all outer coil configurations. A trim coil was included to allow for further manipulation of the magnetic field structure.

[1] Associate Technical Staff, Propulsion Sciences Department, Brendan.M.Plecque@aero.org
[2] Senior Scientist, Propulsion Sciences Department, Mark.W.Crofton@aero.org
[3] Research Scientist, Propulsion Sciences Department, Kevin.D.Diamant@aero.org
[4] Laboratory Manager, Propulsion Sciences Department, Rostislav.Spektor@aero.org
[5] Member of Technical Staff, Propulsion Sciences Department, Jason.A.Young@aero.org
[6] Associate Technical Staff, Propulsion Sciences Department, William.A.Cox@aero.org

Nomenclature

A_e	=	discharge chamber exit area
α	=	thermal expansion coefficient
B	=	magnetic field
D	=	discharge chamber depth
η_b	=	beam efficiency
I_b	=	beam current
I_d	=	discharge current
L	=	arbitrary length
L_i	=	initial length
$\dot{P}$	=	power flux out of discharge chamber
P_a	=	power lost to the anode
P_b	=	beam power
P_{in}	=	input power
P_{ion}	=	ionization power
P_R	=	radiative power loss
P_w	=	power lost to discharge chamber walls
r_{avg}	=	discharge chamber average radius
$r_{chamber}$	=	discharge chamber width to depth ratio
r_i	=	discharge chamber inner radius
r_o	=	discharge chamber outer radius
V_d	=	discharge voltage
V_b	=	beam voltage
T	=	temperature
T_e	=	electron temperature
T_{eV_a}	=	electron temperature at anode
w	=	discharge chamber width

I. Introduction

DUE to the high cost of spacecraft and launch vehicles, increasing payload capacity is very important to the space industry. Larger volume and mass can be reserved for the payload if the satellite bus can be reduced, and electric propulsion has emerged as an attractive way to achieve this. Electric thrusters exhibit about an order of magnitude increase in specific impulse over chemical thrusters, allowing for less volume and mass taken up by propellant. Although electric propulsion consists of multiple types of devices, the focus here will be on the design of a 3-6kW laboratory Hall thruster, intended as a tool for probing device physics. Hall devices in this power class are relatively new to space usage with flight experience on satellites just in the last five years. They are of much interest due to their simple and compact design, high thrust to power ratio at low specific impulse, and efficiency exceeding 50%[1,2].

II. Thruster Design

Hall thrusters are a commonly used type of electrostatic propulsion device. They are routinely employed for station keeping, attitude control, and have recently been used for orbit raising. However, experimental studies in vacuum chambers have shown that Hall characteristics can vary significantly with background pressure[3], magnetic field configuration, component composition and geometry. With the more prominent role that they have in the modern space industry, it is imperative that the relationship between performance in test facilities and on orbit is thoroughly understood. Experimentation within vacuum chambers is a long and tedious process as the chamber must be vented and opened up for any experimental changes to be made. As a result of this, it was desired that a variable geometry medium power Hall thruster be designed and constructed for experimentation. The thruster was named AM-1.

A. Basic Function of a Hall Thruster

There are two general types of Hall thrusters, the stationary plasma thruster (SPT) and thruster with anode layer (TAL). Only the more common SPT type will be considered in this paper. The SPT consists of a cylindrical channel of dielectric material with anode located on the interior, solenoids and ferromagnetic pole pieces that create a primarily radial magnetic field, and a cathode located external to the channel. It is an electrostatic propulsion device that uses magnetic and electric fields to ionize xenon propellant, accelerate ions, and create thrust[2]. Diagrams showing the

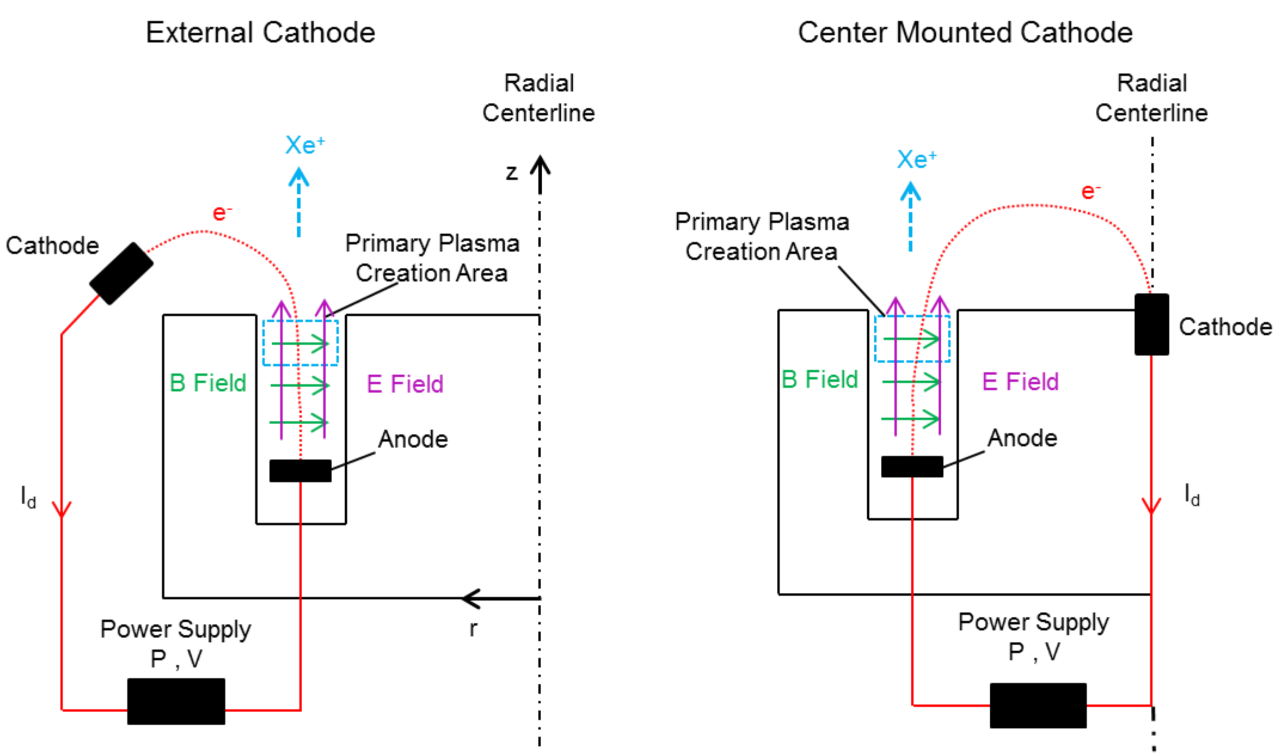

Figure 1. Cross section of Hall thruster with external and center mounted cathode locations

coordinate system used and the typical structure of an SPT-type design with the cathode in two positions are shown in Figure 1.

The xenon gas propellant enters the discharge chamber through the anode, while electrons are emitted from the cathode and travel towards the anode. Once the electrons come in contact with the crossed E and B fields, they begin to travel azimuthally around the annular discharge chamber where they collide with and ionize the xenon neutrals. The newly created xenon ions are then accelerated out of the discharge chamber due to the electric field, producing thrust.

It was desired that the thruster being designed (AM-1) perform similarly to current thrusters within the 3-6kW range so that it could be used to diagnose their issues and further investigate their phenomena. Specific dimensions selected to achieve this while providing the desired capabilities are shown in Table 1. CAD models showing the minimum and maximum translation are shown Figure A1 in the Appendix.

Table 1. AM-1 dimensions

Variable	Name	Value	Units
w	Chamber width	21	mm
D	Chamber depth	18 – 58	mm
r_o	Chamber outer radius	97	mm
r_{avg}	Chamber average radius	76	mm
r_i	Chamber inner radius	55	mm
A_e	Chamber exit area	20,056	mm^2

B. Magnetic Field Structure

A problem with current Hall thrusters is that the high energy ions diverge at the exit of the thruster, and at times bombard the walls of the discharge chamber. An approach to solve this problem, now referred to as magnetic shielding has been developed. It manipulates the electric and magnetic field structure to focus the particles towards the center of the discharge chamber and maintain high electric potential along the discharge chamber wall[4]. This increases the ion axial velocity and overall thruster efficiency and reduces the ion flux to the chamber walls, minimizing wall erosion. A diagram comparing the magnetic field structure of unshaped and magnetically shielded configurations is shown in Figure 2.

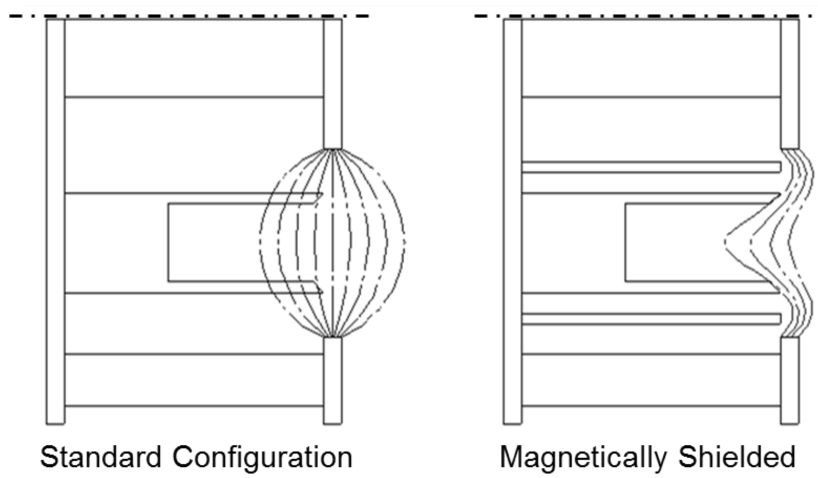

Figure 2. Magnetic field comparison of standard configuration and magnetically shielded configuration

Further exploration of this topic determined that the following two criteria must be met to achieve magnetic shielding[5]. The first criterion can be seen in the magnetic field configurations shown in Figure 2. The B-field lines must have concavity that curve around the discharge chamber. The second criterion has to do with the electric potential associated with each B-field line. Within the primary plasma creation region in Hall thrusters, there is very low variation in potential along the B-field lines[4]. Therefore, they can be thought of as contour lines of electric potential with the magnitude increasing as it approaches the anode at the base of the discharge chamber. In order to meet the second criterion, the potential on the line tangent to the discharge chamber walls must correspond closely with the potential at the anode. If both of these criteria are met, the thruster is said to be magnetically shielded. The steps taken to achieve this magnetic field design will be discussed later in the report.

C. Initial Sizing

Current Hall thruster designs for the power class of interest include P5, H6, SPT-140 and BPT-4000 (XR-5) devices. In order to capture the essential physical characteristics of modern Hall thrusters, current designs were considered in this study. The P5 was used as a base and was modified to create a device that fit all the desired functions[6]. The AM-1 was designed to operate from 2-6 kW at discharge voltages of about 300-400V. The discharge chamber was sized to allow for a minimum power density, $\dot{P}$, approximately equal to the BPT-4000 minimum at 3kW. The power density is given by equation 1

$$\dot{P} = {P_{in}}/{A_e} \tag{1}$$

where P_{in} is the input power and A_e is the exit area of the discharge chamber. AM-1 power density is similar to others in the power class of interest. Structural constraints from the inner coil design resulted in the AM-1 chamber inner radius being chosen to be 55 mm. In order to match the power density, the outer radius was chosen to be 97 mm. The width to depth ratio of the annular discharge region, $r_{chamber}$, was used to size the depth, D, of the chamber and is given by equation 2

$$r_{chamber} = {w}/{D} = {(r_o - r_i)}/{D} \tag{2}$$

where w is the width of the annulus, r_o is the outer radius, and r_i is the inner radius. In typical thrusters, $r_{chamber}$ is about 0.8-0.9. Since the AM-1 will have a translatable anode, it was desired that the $r_{chamber}$ values encompass this regime. Consequently, D was chosen to be 58 mm in the most rearward position, corresponding to $r_{chamber}$ ~0.7. By translating the anode forward up to 40mm, this value can be anywhere between 0.36 and 1.17.

D. Power Dissipation Analysis

A simple power dissipation analysis was performed to predict where the input power would be expended at a given discharge voltage V_d and discharge current I_d[2,7]. P_{in} is split up into five components, shown below in equation 3

$$P_{in} = P_b + P_w + P_a + P_R + P_{ion} \tag{3}$$

Here P_b is the power into the ion beam, P_w is the power lost to the channel walls due to ion collision and thermalization, P_a is the power lost to the anode due to collection of electrons, P_R is the radiative power loss from the plasma, and P_{ion} is power that goes into ionization of the xenon. It is important to note that for this basic analysis P_R was neglected due to its small relative magnitude.

The beam power was estimated using equation 4

$$P_b = P_{in}\eta_b \tag{4}$$

Here η_b is the non-dimensional beam efficiency, which was assumed to be 0.8 from the known value of the NASA 173Mv2 Hall thruster of similar size and power2. The power to the walls was estimated using equation 5, which assumes that the axial electric field ten times the radial electric field. This is typical of thrusters this size.

$$P_w = 0.485 I_b V_b \tag{5}$$

Here I_b is the beam current given by $I_d\eta_b$ and V_b is the beam voltage given by $V_d\eta_b$. P_a is calculated by equation 6

$$P_a = 2 I_d T_{eV\_a} \tag{6}$$

Where T_{eV_a} is the electron temperature at the anode, which was assumed to be 10% of the 25eV plasma electron temperature. P_{ion} can be estimated using equation 7

$$P_{ion} = 0.09 I_b V_b \tag{7}$$

Based on the assumption that η_b is 0.8 and the ionization potential is 5% of the beam voltage[2]. The calculation of these values allows for further modeling to be done. The maximum values are tabulated in Table 2.

Table 2. Max value of each component of power within P_{in} of 6000 W and V_d of 300-400 V

Component	Symbol	Power [W]	Input Power [W]	Discharge Voltage [V]
P_b	Beam Power	4800	6000	300
P_w	Power to Wall	1862	6000	300
P_a	Power to Anode	100	6000	300
P_{ion}	Ionization Power	230	6000	300

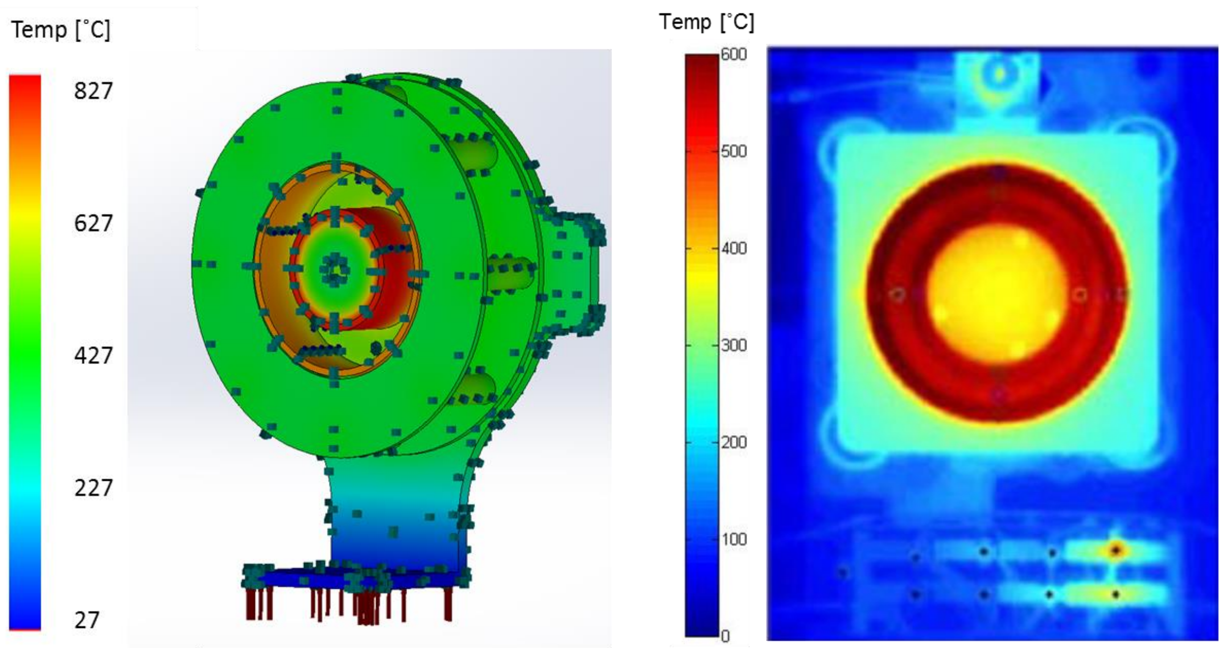

Figure 3. Comparison of SolidWorks Thermal Analysis for 6kW 300V Hall thruster to IR camera temperature measurement of BPT4000 thruster at 4.5kW 400V (ref 8)

E. Thermal Modeling

Basic thermal modeling was performed on the thruster to ensure that high temperature during operation would not be an issue. The SolidWorks Simulation Professional Thermal Analysis add-on was used. In order to minimize the computing power needed and time to run each simulation, the CAD model geometry was simplified and holes were removed. It was assumed that the power to the wall was 1,862 W and power to the anode was 100 W. These correspond to the maximum values from the power dissipation analysis previously described. An image of the simulation is shown next to an image from an IR camera measurement device[8] of a 4.5kW and 400V Hall thruster operating below.

The component of interest is the boron nitride discharge chamber, which has the highest heat flux due to the large amount of power lost to the walls from ion collisions. It can be seen that the BPT4000 thruster reaches a temperature

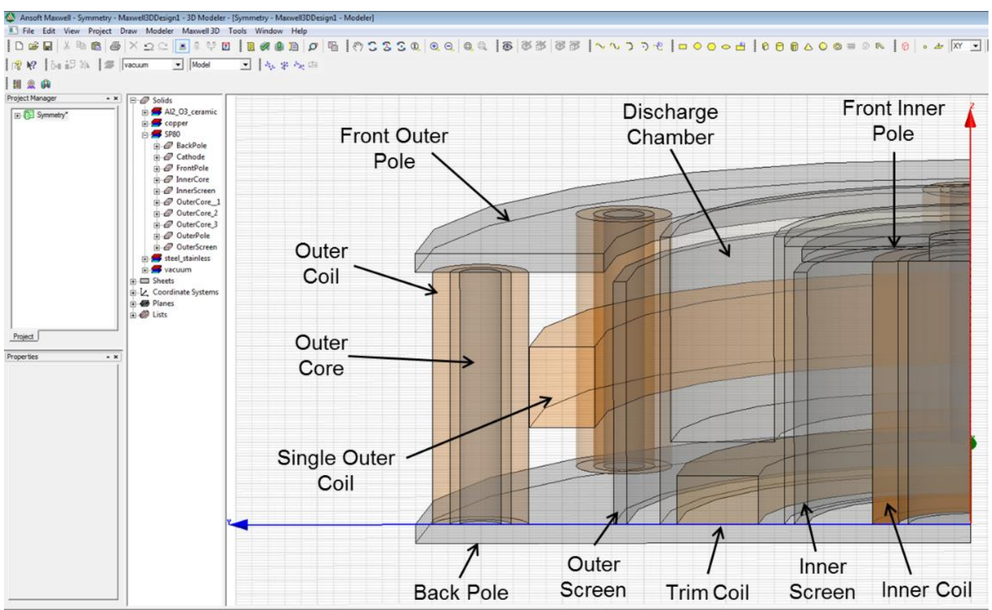

Figure 4. Screenshot of Maxwell 3D interface with thruster components labeled

of about 600˚C while firing[8] and the 6kW, 300V thruster reaches about 800˚C in the simulation. The increase in temperature was to be expected because the input power is different between the two cases. This was used as a sanity check to ensure that the estimates from the thermal modeling and power dissipation simulation were valid. Additionally, it has been shown that the boron nitride discharge chamber of the PPSX000-ML thruster can withstand temperature of 800˚C[9]. From this, it was deduced that the high boron nitride temperature would not cause failure of thruster components.

F. Magnetic Field Design

The magnetic field design was performed using ANSYS Maxwell 3D electrostatic simulation software. To do this, multiple assumptions and simplifications having to be made. To speed up computing time, only a quarter of the thruster was included and symmetry boundary conditions were used. A custom material with a relative permeability of 1,000 was made to match the magnetic properties of high purity cast iron. The coil windings were modeled as a solid piece of copper and a current equal to the product of the wire current and amount of turns was run through it. A screenshot of the interface with CAD model is shown in Figure 4.

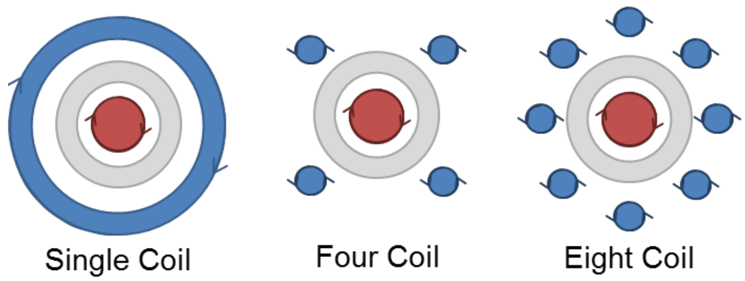

Figure 5. Different outer coil configurations. Note that blue, grey, and red correspond to outer coil, discharge chamber, and inner coil respectively

The effects of adding axial screens, a trim coil behind the discharge chamber, and implementing different outer coil configurations were investigated.

1. Outer Coil Configuration

The outer coil configuration varies between thrusters, although each is able to produce a similar radial magnetic field within the chamber. Some thrusters have eight outer coils, some have four outer coils, and some have a single outer coil. Specifically, the P5 and H6 have eight outer coils, the BPT-4000 and BHT-8000 have four coils, and the NASA 173Mv2 has a single outer coil. These configurations are shown below in Figure 5.

In order to better understand the benefit of each type, the thruster was designed to allow for the possibility of each configuration. Each coil was sized to produce the desired radial magnetic field component within the chamber. The addition of these coils caused some design changes within the thruster. The total thruster diameter was increased from 12.5” to 13.8” to accommodate for the single outer coil. A cross sectional diagram showing the outer coil mounting schemes is shown in Figure 6.

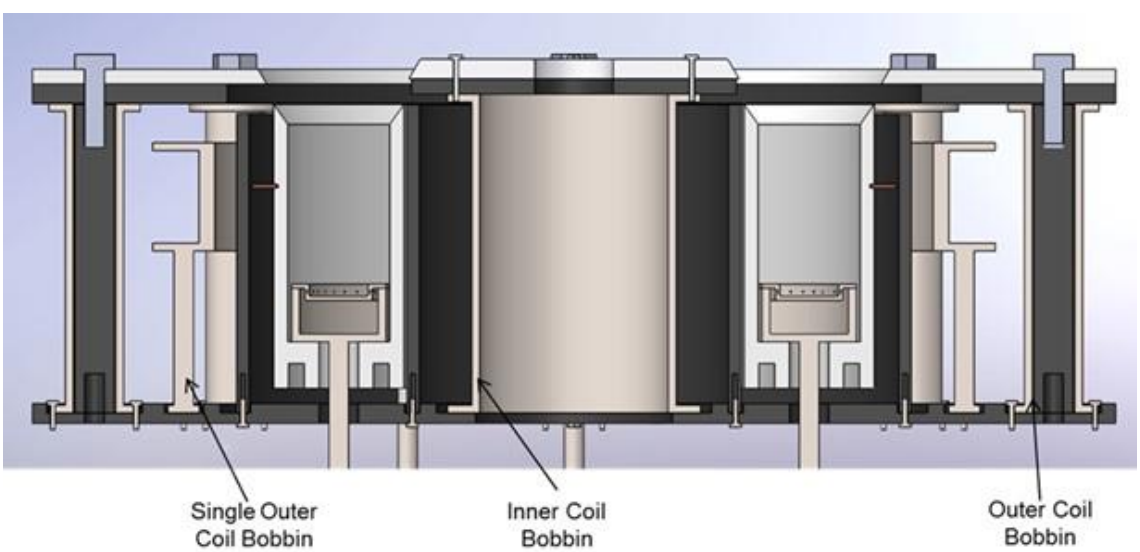

Figure 6. CAD cross section of AM-1 with magnetic circuit labelled.

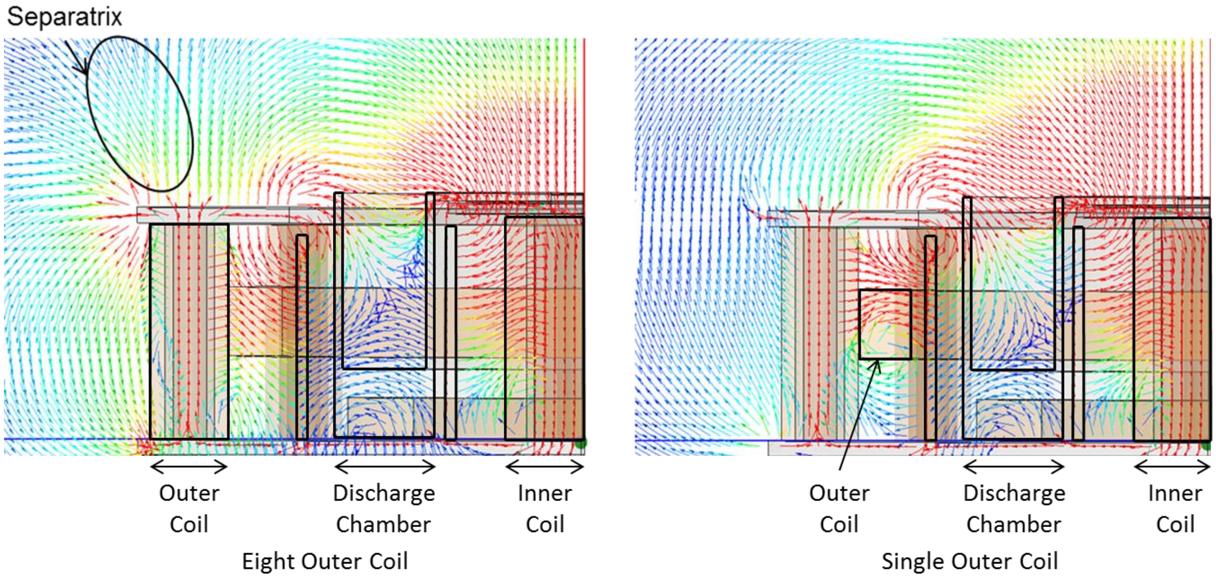

Figure 7. Magnetic field of thruster for eight outer coil vs single outer coil configurations

Although the magnetic field within the discharge chamber looks very similar (it is mainly a function of pole geometry), the magnetic field exterior of the thruster for the single coil configuration is very different from the others. The four and eight coil configurations produce a separatrix of the magnetic field outside of the thruster, which is shown in Figure 7. The ability to create the same discharge chamber B-field while varying exterior B-field will allow for the benefits and disadvantages of each outer coil configuration to be characterized.

The eight coil configuration also allows for azimuthal asymmetry to be created within the discharge chamber to investigate its effects on the thruster performance. This is done by running the current in each successive coil in an opposite direction. The magnetic field from each outer magnet will be in the opposite direction and cancel out. A plot showing the potential B-field variability is shown in Figure 8 for all coils running the same direction, 4 coils running the same direction, and successive coils running in the opposite direction. The jagged lines are due to the computer not being able to run the simulation for a fine mesh. It is important to note that there is less than 1% fluctuation in Br for the eight coil current same direction case.

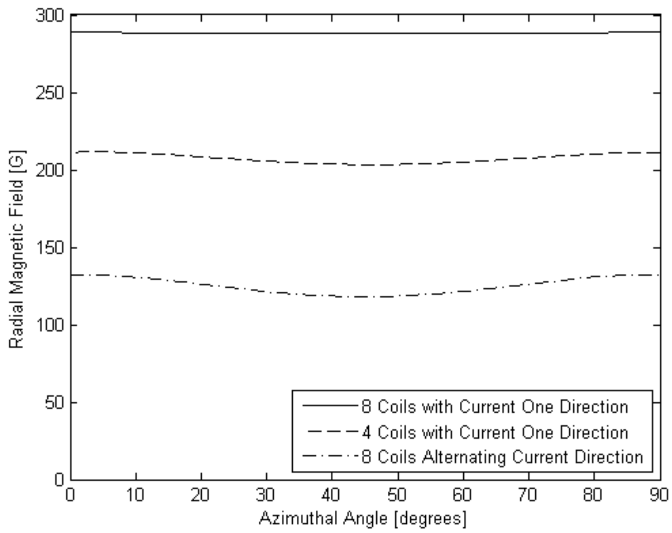

Figure 8. Mid channel Br at the exit plane for different outer coil currents

2. Axial Screens

Axial Screens were added to further manipulate the magnetic field. Their addition creates concavity of the magnetic field lines which is necessary for magnetic shielding. A diagram showing the basic geometry of axial screens is shown in Figure 9.

A screen length of 97 mm and a distance to exit of 3 mm was chosen for the AM-1 based on their chamber magnetic field geometry. The inner screen length and the outer screen length are equal. Below in Figure 10, mid discharge chamber radial magnetic field and axial magnetic field are plotted against axial distance for different axial screen lengths.

It can be seen that as NXX increases, dBr/dz within the chamber increases. Along with this comes a decrease in Brmax and negative shift in peak location, while the field downstream of the peak shows minimal change. A magnetic field vector map in a cross sectional plane of the thruster is shown below in Figure 11 for configurations with and without axial screens.

Despite the addition of axial screens slightly decreasing Brmax, they create concavity of the magnetic field lines within the discharge chambers. B field line concavity is a fundamental part of creating a magnetically shielded discharge chamber.

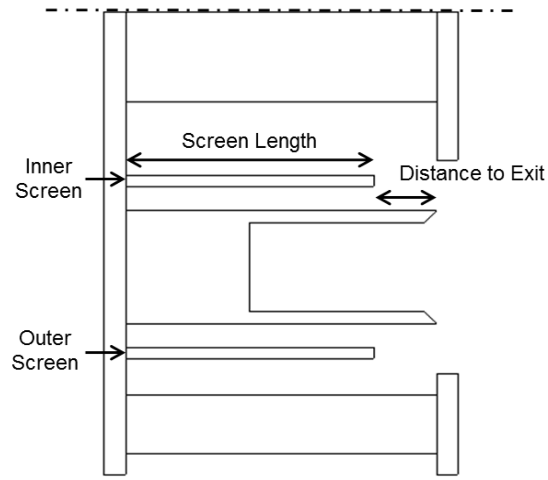

Figure 9. Cross Sectional diagram showing axial screens

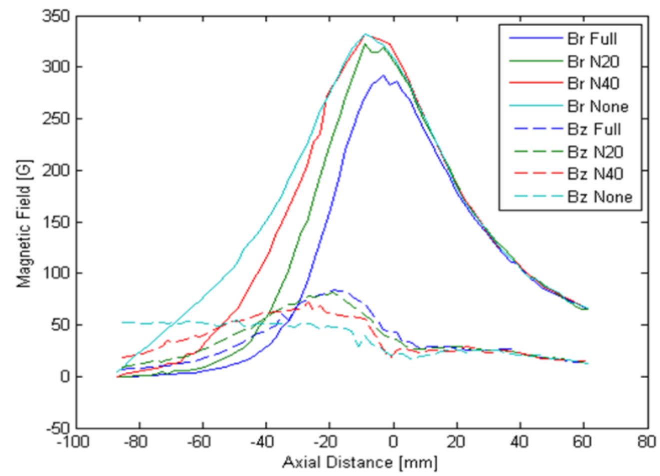

Figure 10. Effect of axial screen length on mid channel radial and axial magnetic field. NXX corresponds to a decrease in screen length of XX mm. The discharge chamber exit is at 0mm.

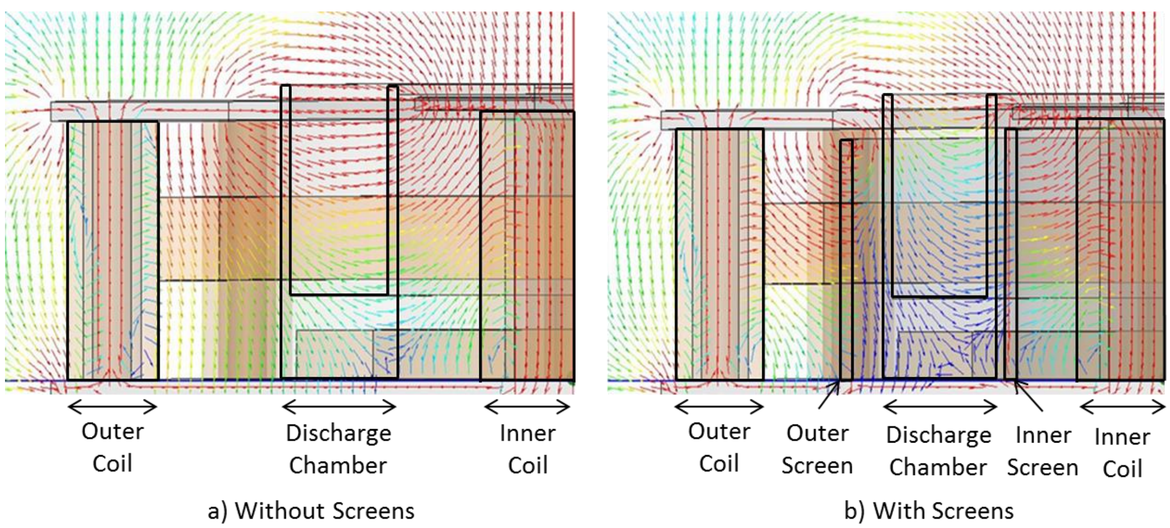

Figure 11: Visualization of the magnetic field change due to axial screens

3. Trim Coil

To allow for further manipulation of the magnetic field, a trim coil was added beneath the discharge chamber[10]. This has been used in multiple thrusters including the magnetically shielded SPT100M[11]. When activated, the trim coil counteracts the radial component of magnetic field towards the base of the discharge chamber without having a large effect on the radial magnetic field towards the thruster exit plane. This increases dBr/dz and creates greater concavity of field lines within the thruster. It also creates symmetry of the magnetic field lines about the center of the discharge chamber, resulting in both the inner and outer wall being shielded. The qualitative effect on magnetic field lines and quantitative effect on radial magnetic field of the trim coil is shown below in Figures 12 and 13.

The pole geometry and electromagnet strength were varied to create a magnetic field similar to that of the magnetically shielded SPT100M. As shown in figure 9, the addition of a trim coil current decreases the radial magnetic field towards the base of the thruster, while leaving Br max constant. This creates a magnetic field very similar to that of the SPT100M.

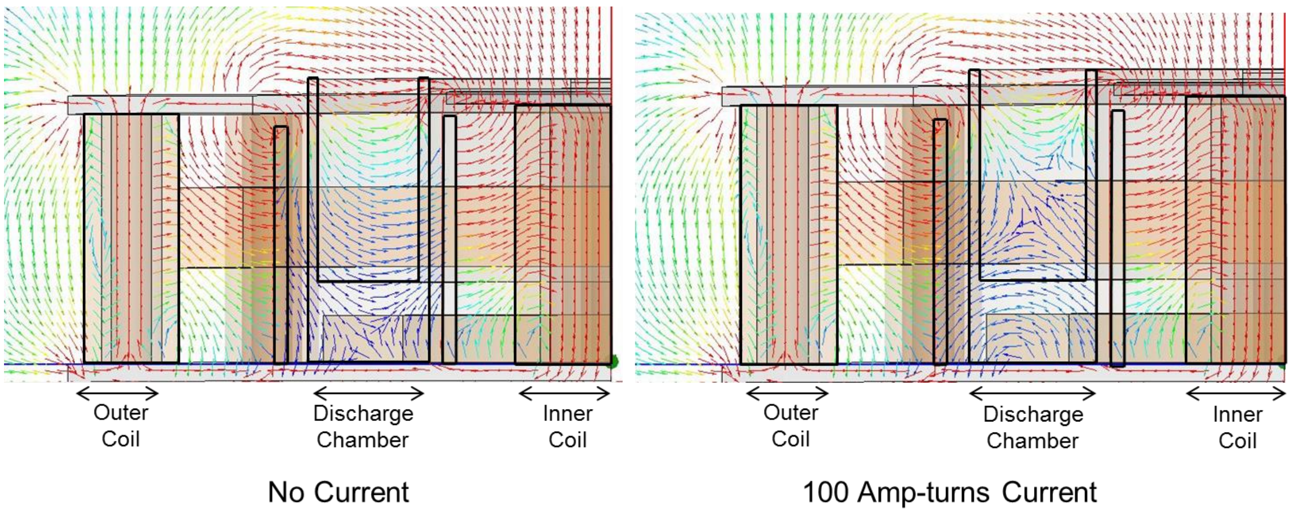

Figure 12: Contour plots of magnetic field vectors for 0 and 100 amp-turns trim current

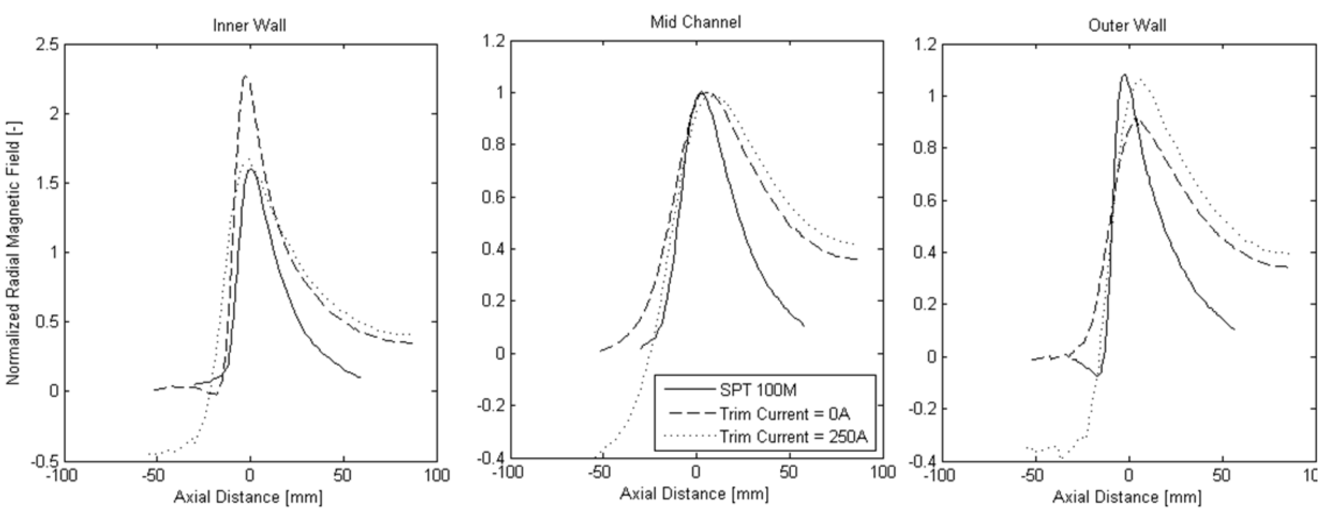

Figure 13. Comparison of radial magnetic field of current thruster for 0 and 250 amp-turns trim current (TC) and SPT100m at multiple radial positions in thruster. The discharge chamber exit is at 0mm (ref 11).

G. Translatable Anode

It was desired that the anode be able to translate axially in vacuum within the discharge chamber in order to investigate how its position affects thruster performance. Typically, Hall thruster scaling rules use a fixed ratio of chamber width to chamber depth (effectively depth of anode). However, these scaling parameters are not absolute, prompting this study. The mechanism for anode translation is shown in Figure 14.

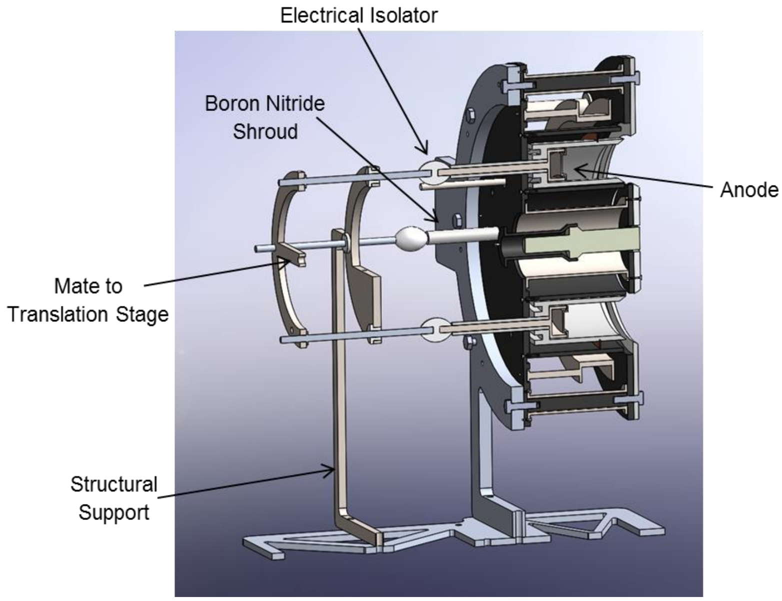

Figure 14. Cross section showing anode translation mechanism

The rods running out the back of the thruster connected to the anode are covered by a boron nitride shroud to prevent plasma formation around them; due to their high potential. They will mount to electrical isolators which will be connected via a rod to structural support and the translation stage. The anode will be able to translate 50mm axially, corresponding to a discharge chamber width to depth ratio of 0.7 to 2.0, which covers the range of most thrusters that have width to depth ratios of 0.8-0.9.

H. Translatable Discharge Chamber

Another desired capability of the thruster is to have the discharge chamber translate axially while under vacuum. This allows for experimental studies varying the location of Br max relative to the exit plane and would also allow for the discharge chamber to be strategically aligned so its walls are tangent to the electric potential line that corresponds to the maximum that the ions and electrons can reach. This gives the thruster the ability to meet both magnetic shielding criteria. However, this is quite difficult to achieve mechanically. One complication is that it is desired that the side of the discharge chamber is not covered so laser diagnostics and thermocouple measurements can be made in the chamber after swapping the discharge chamber with one containing a side port. The discharge chamber will be made out of boron nitride for its dielectric and thermal properties. The chamber support and rods that connect to the translation stage were chosen to be made out of aluminum for its structural properties. This creates an issue in mating the two because the thermal expansion coefficients are very different and the boron nitride is very susceptible to cracking. To solve this problem, a chamber support holder and copper ring fixtures were designed out of aluminum and copper, respectively. A CAD model is shown in Figure 15.

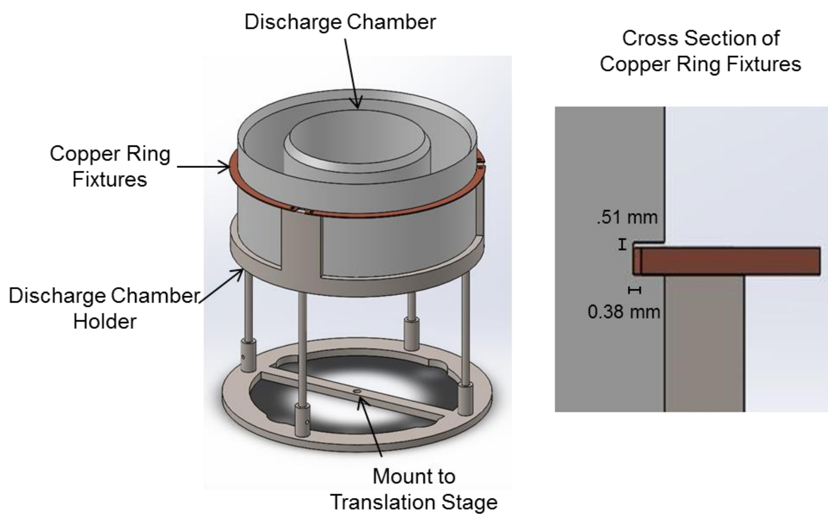

Figure 15. Discharge Chamber holder and cross section of copper ring

The aluminum discharge chamber holder will provide the majority of the support for the discharge chamber. It is connected directly to the translation stage. In order to fix the discharge chamber in the holder, copper ring fixtures were designed to fit into a groove in the discharge chamber boron nitride. Linear thermal expansion was assumed the thermal expansion of each component was found using equation 8

$$\Delta L = \alpha L_i \Delta T \tag{8}$$

Where ΔL is the length change, L_f is the final length, L_i is the initial length, α is the thermal expansion coefficient, and ΔT is the temperature change. It was found that when heated 800˚C, the boron nitride would expand .004 mm and 0.001 mm in radius and channel length and the copper would expand 1 mm in radius and .013 mm in thickness. The above spacing will allow for the outward expansion of these materials. Additionally, the malleability of copper will reduce the chance of fracturing the boron nitride.

I. Comparison to Current Thrusters

Using magnetic field data attained experimentally and through certain technical papers, a comparison was made between the designed Hall thruster and the P5 Hall thruster. A plot of mid channel radial magnetic field versus axial distance is shown in Figure 15 for all of these thrusters. Additionally, the shift in radial magnetic field attainable by the translation stage mechanism is shown. This illustrates how the translation of the chamber can change the magnetic field relative to the exit plane.

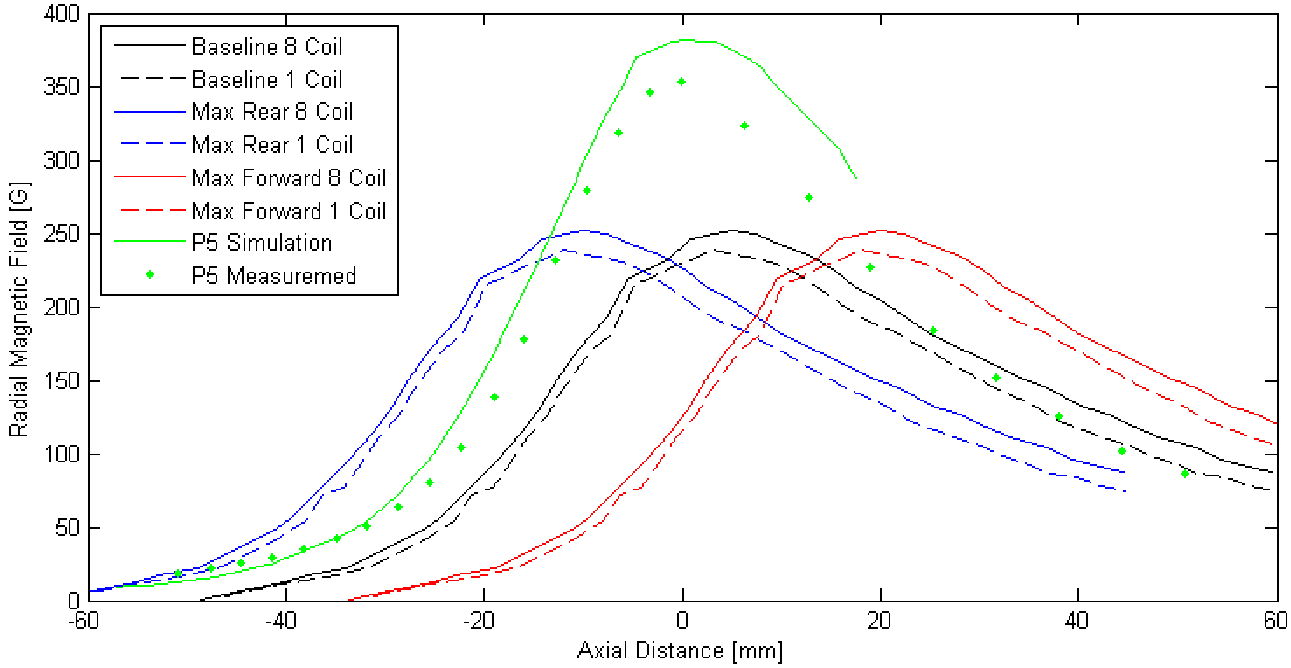

Figure 16. Mid channel radial magnetic field comparison to P5. The discharge chamber exit is at 0mm.

III. Conclusion

In conclusion, a variable geometry Hall thruster was developed for experimentation. The adjustable electromagnets will allow for investigating the effects of magnetic field azimuthal asymmetry, external separatrix, and different outer coil configurations on thruster performance. The translatable discharge chamber and anode will allow for investigation of magnetic shielding, discharge chamber sizing, and location of exit plane relative to magnetic field. The variable location cathode will allow for experimentation on how the cathode's position will affect thruster performance. The results of experiments on this device can be extrapolated to learn more about Hall thruster operation and solve issues with thrusters currently in use.

Appendix

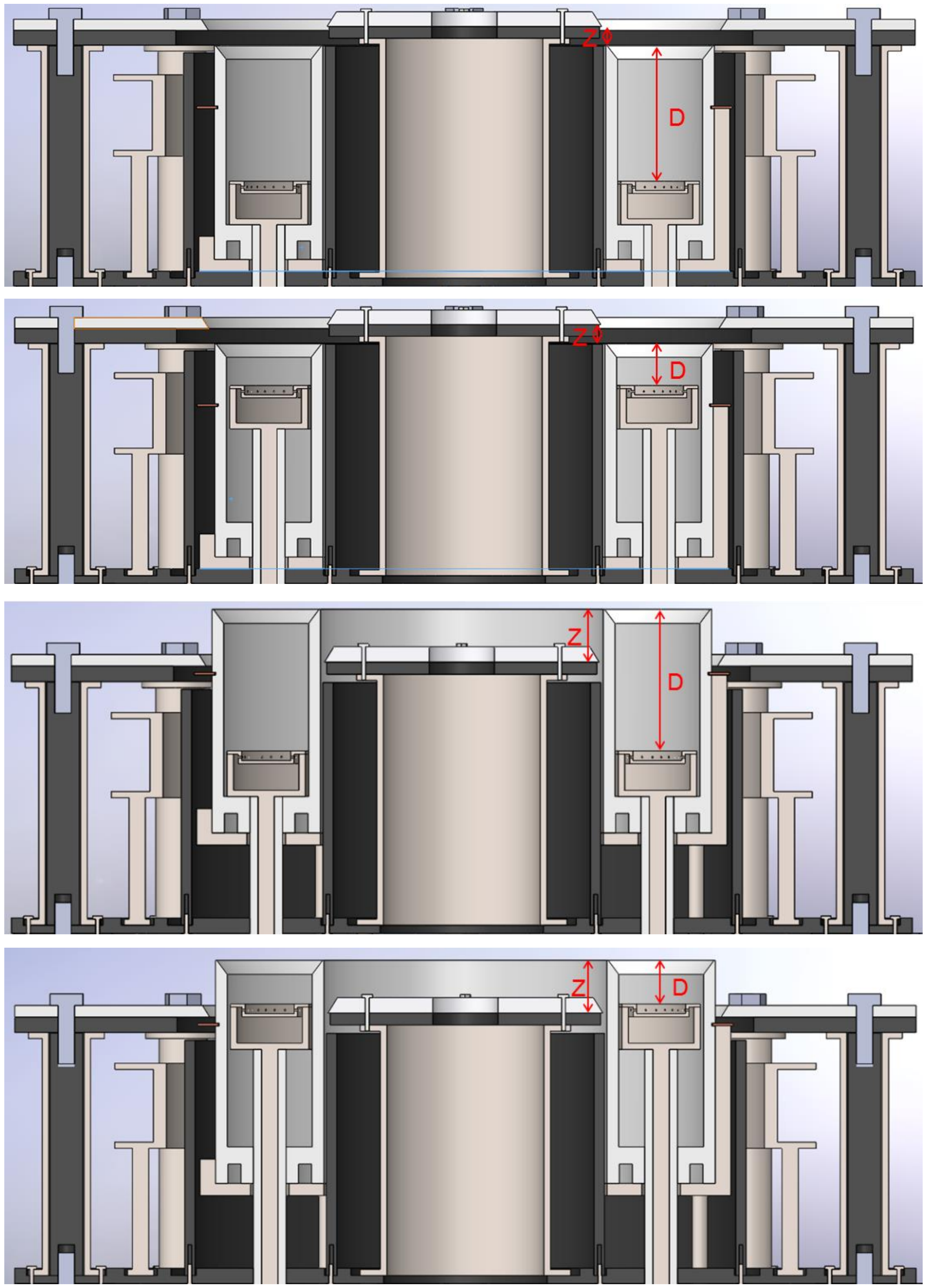

Figure A1. CAD model showing cross sectional view of the possible anode and discharge chamber locations

Table A1. Anode and discharge chamber positions corresponding to the views of Figure A1

Image	Anode Position	D [mm]	Chamber Position	Z [mm]
a	Max Rearward	58	Max Rearward	-7
b	Max Forward	18	Max Rearward	-7
c	Max Rearward	58	Max Forward	23
d	Max Forward	18	Max Forward	23

References

[1]Byers, D.C., and Dankanich, J. W., "Geosynchronous Earth Orbit Communication Satellite Deliveries with Integrated Electric Propulsion" *Journal of Propulsion and Power*, Vol. 24, No. 6, pp. 1369-1375

[2]Goebel, Dan M., and Ira Katz. *Fundamentals of Electric Propulsion Ion and Hall Thrusters*. John Wiley and Sons Inc. Hoboken, NJ 2008

[3]Nakles, Michael R. "Background Pressure Effects on Ion Velocity Distribution Within a Medium-Power Hall Thruster." *Journal of Propulsion and Power*, Vol. 27, No. 4, pp. 737-743

[4]King, David Q., Kristi H. De Grys, Randall S. Aadland, Dennis L. Tilley, and Arnold W. Voigt. Primex Aerospace Company, Redmond, WA, U.S. Patent Application for "Magnetic Flux Shaping in Ion Accelerators with Closed Electron Drift." No. 6,208,080 B1. 27 Mar. 2001.

[5]Mikellides, I. G., Katz I., Goebel, D. M., Hofer, R. R. "Magnetic Shielding of the Channel Walls in a Hall Plasma Accelerator." *Physics of Plasmas, Vol 18. 033501 (2011)*

[6]Gulczinski, Frank S. *Examination of the Structure and Evolution of Ion Energy Properties of a 5 kW Class Laboratory Hall Effect Thruster at Various Operational Conditions*. Diss. U of Michigan, 1999.

[7]Martinez, R., Dao, H., Walker, M. (2014). Power Deposition into the Discharge Chamber of a Hall Effect Thruster. *Journal of Propulsion and Power,* Vol. 30, No. 1, pp. 209-220

[8]Spektor, R. "Infrared Thermographic Diagnostic for Imaging Hall Thrusters." *International Electric Propulsion Conference*, 452, Washington D.C., 2013

[9]Mazouffre S., Dannenmayer C., Blank C. "Impact of Discharge Voltage on Wall-losses in a Hall Thruster." *Physics of Plasmas, Vol 18*. 064501 (2011)

[10]Hofer, Richard R. *Development and Characterization of High-Efficiency, High-Specific Impulse Xenon Hall Thrusters*. Diss. U of Michigan, 2004.

[11]Mitrofanova, O., Gnizdor, R., & Murashko, V.. "*New Generation of SPT-100*." *International Electric Propulsion Conference*. 041. Wiesbaden, Germany, 2011